

Score-based Diffusion Models with Self-supervised Learning for Accelerated 3D Multi-contrast Cardiac MR Imaging

Yuanyuan Liu, Zhuo-Xu Cui, Congcong Liu, Hairong Zheng, *Senior Member, IEEE*, Haifeng Wang, *Senior Member, IEEE*, Yihang Zhou, and Yanjie Zhu, *Member, IEEE*

Abstract—Long scan time significantly hinders the widespread applications of three-dimensional multi-contrast cardiac magnetic resonance (3D-MC-CMR) imaging. This study aims to accelerate 3D-MC-CMR acquisition by a novel method based on score-based diffusion models with self-supervised learning. Specifically, we first establish a mapping between the undersampled k -space measurements and the MR images, utilizing a self-supervised Bayesian reconstruction network. Secondly, we develop a joint score-based diffusion model on 3D-MC-CMR images to capture their inherent distribution. The 3D-MC-CMR images are finally reconstructed using the conditioned Langervin Markov chain Monte Carlo sampling. This approach enables accurate reconstruction without fully sampled training data. Its performance was tested on the dataset acquired by a 3D joint myocardial T_1 and $T_{1\rho}$ mapping sequence. The T_1 and $T_{1\rho}$ maps were estimated via a dictionary matching method from the reconstructed images. Experimental results show that the proposed method outperforms traditional compressed sensing and existing self-supervised deep learning MRI reconstruction methods. It also achieves high quality T_1 and $T_{1\rho}$ parametric maps close to the reference maps obtained by traditional mapping sequences, even at a high acceleration rate of 14.

Index Terms—3D cardiac magnetic resonance imaging, self-supervised, diffusion models, multi-contrast

I. INTRODUCTION

This study was supported in part by the National Key R&D Program of China nos. 2021YFF0501402, 2020YFA0712200, National Natural Science Foundation of China under grant nos. 62322119, 62201561, 62206273, 12226008, 62125111, 62106252, 81971611, and 81901736, the Guangdong Basic and Applied Basic Research Foundation under grant no. 2021A1515110540, and the Shenzhen Science and Technology Program under grant no. RCYX20210609104444089. (Corresponding author: Yanjie Zhu)

Yuanyuan Liu, Congcong Liu, Hairong Zheng, Haifeng Wang and Yanjie Zhu are with Paul C. Lauterbur Research Center for Biomedical Imaging, Shenzhen Institute of Advanced Technology, Chinese Academy of Sciences, Shenzhen, Guangdong, China (e-mail: {liuyy; cc.liu; hr.zheng; hf.wang1; yj.zhu}@siat.ac.cn).

Zhuo-Xu Cui, Yihang Zhou are with Research Center for Medical AI, Shenzhen Institute of Advanced Technology, Chinese Academy of Sciences, Shenzhen, Guangdong, China (e-mail: {zx.cui; yh.zhou2}@siat.ac.cn).

Congcong Liu is also with Shenzhen College of Advanced Technology, University of Chinese Academy of Sciences

Yuanyuan Liu and Zhuo-Xu Cui contributed equally to this study.

MYOCARDIAL parameter mapping, including T_1 , $T_{1\rho}$, T_2 , and T_2^* mapping, is an important technique in cardiovascular MR imaging (CMR). It enables the quantification of MR relaxation times, serving as biomarkers for a range of cardiac pathologies [1]. In contemporary CMR, there is a growing emphasis on characterizing multiple relaxation times simultaneously through the acquisition of multi-contrast (MC) images. Examples include joint myocardial T_1 and T_2 mapping [2], cardiac MR fingerprinting (MRF) [3], and CMR multitasking [4]. Furthermore, 3D-CMR can provide information of whole-hearts relative to 2D imaging with limited coverage, but it suffers from the long scan time, especially for multi-parameter mapping [5]. Therefore, accelerated 3D multi-contrast imaging of CMR is highly desirable for practical use.

One major strategy to accelerate 3D-MC-CMR is undersampling the k -space data and subsequently reconstructing images from this undersampled data using regularized techniques with hand-crafted priors. Various priors have been employed in 3D-MC-CMR reconstruction, such as subspace modeling [6], patch-based [7], [8], and tensor-based low-rankness [9]. These approaches can achieve high acceleration rates while maintaining high reconstruction quality. However, constructing priors is non-trivial, and the iterative nature of these methods leads to time-consuming computations. Deep learning (DL) has emerged as a successful tool in MR reconstruction, reducing computational complexity and enhancing reconstruction quality. However, most DL-based reconstruction methods rely on supervised learning that requires extensive fully sampled datasets for training. Acquiring high-quality, fully sampled k -space data is challenging for 3D-MC-CMR since the scan time is extremely lengthy. Moreover, respiratory or heart rate instability may occur during the prolonged scan time of 3D-MC-CMR imaging, resulting in a degradation of image quality. Therefore, these supervised learning methods are unsuitable for accelerating 3D-MC-CMR.

To address this issue, self-supervised learning methods have been adopted. One strategy directly reconstructs images from the undersampled k -space data by enforcing the data consistency using the physical model in the reconstruction [10], [11]. Another strategy is training the networks with a sub-sample of the undersampled k -space data acquired. A notable example is the self-supervised learning via data undersampling (SSDU) method [12]. SSDU divides the measured data into

two distinct subsets: one for use in the data consistency term of the network, and the other to compute the loss function. Consequently, network training can be completed using only undersampled data. Based on SSDU, the reference [13] trains the network in both k -space and image domain and applies it in accelerated non-cartesian MRI reconstruction.

Recently, the score-based diffusion model [14], [15] has been applied to MR reconstruction and has shown promising results in reconstruction accuracy and generalization ability. It learns data distribution rather than end-to-end mapping using the network between undersampled k -space data and images, and therefore is recognized as an unsupervised learning method for solving inverse problems of MR reconstruction. Specifically, it perturbs the MR data distribution to a tractable distribution (i.e. isotropic Gaussian distribution) by gradually injecting Gaussian noise, and one can train a neural network to estimate the gradient of the log data distribution (i.e. score function). Then the MR reconstruction can be accomplished by sampling from the data distribution conditioned on the acquired k -space measurement. Although treated as an unsupervised technique [16], score-based reconstruction still needs amounts of high-quality training images to estimate the score function. The image collection is also challenging for 3D-MC-CMR. A simple and straightforward strategy to solve this issue is using the reconstruction results of traditional regularized or self-supervised learning methods as training samples. However, the residual reconstruction errors may lead to discrepancy in the data distribution of diffusion models. Previous studies have shown that Bayesian neural networks predict the target with uncertainty by training the networks with random weights, provide a more comprehensive sampling over the whole distribution and may avoid the discrepancy [17].

In this study, we sought to develop a self-supervised reconstruction method for 3D-MC-CMR using the score-based model with a Bayesian convolutional neural network (BCNN). Specifically, a self-supervised BCNN was developed based on the neural network driven by SPIRiT-POCS model [18]. Then the score-based model was trained by the samples over the network parameter distribution of BCNN. To better utilize the correlations among MC images, we used a joint probability distribution of MC data instead of the independent distribution in the original score-based model. The proposed method (referred to as "SSJDM") was tested using the data acquired by a 3D joint myocardial T_1 and $T_{1\rho}$ mapping sequence [2], [19]. It outperformed the state-of-the-art methods, including regularized and self-supervised DL reconstructions, at a high acceleration rate (R) of up to 14. The obtained T_1 and $T_{1\rho}$ values were also comparable with the traditional 2D myocardial parameter mapping methods.

II. MATERIAL AND METHODS

A. Background

Suppose the MR image, denoted as \mathbf{x} , is a random sample from a distribution $p(\mathbf{x})$, i.e., $\mathbf{x} \sim p(\mathbf{x})$. To sample \mathbf{x} from $p(\mathbf{x})$, we can use the Langevin Markov Chain Monte Carlo (MCMC) sampling method in practical use [20]. In accelerated

MRI, only the undersampled k -space data, denoted as \mathbf{y} , can be obtained and therefore accessing the distribution $p(\mathbf{x})$ is challenging. Fortunately, we can assume the existence of a mapping from the measurements \mathbf{y} to the image \mathbf{x} , expressed as $\mathbf{x} = \mathbf{f}_\theta(\mathbf{y}) + n$. \mathbf{f}_θ represents a mapping parameterized by θ , where θ follows a distribution $p(\theta)$, i.e., $\theta \sim p(\theta)$, and n denotes Gaussian noise. Statistically, $p(\theta)$ can be approximated by a distribution $q(\theta)$ through variational inference accomplished using BCNN. Then by substituting the learned $q(\theta)$ into the mapping mentioned above, we can employ the score-matching technique to estimate the score of $p(\mathbf{x})$, i.e. the gradient of $\log p(\mathbf{x})$, allowing the implementation of Langevin MCMC sampling.

1) *Bayesian convolutional neural network*: BCNN is a type of neural network that combines traditional CNN architectures with Bayesian methods for uncertainty estimation, belonging to stochastic artificial neural networks [17]. Specifically, it treats each weight parameter in CNNs as a random variable following a prior distribution, typically Gaussian distribution. BCNN learns the distributions of the weights, which can be used to quantify the uncertainty associated with the probabilistic predictions.

To design a BCNN, the first step is choosing a CNN \mathbf{f}_θ as the functional model, with its weights represented as θ , and establishing a prior distribution for the model's parameters, denoted as $p(\theta)$. This process can be formulated as follows:

$$\mathbf{x} = \mathbf{f}_\theta(\mathbf{y}) + \epsilon, \quad \theta \sim p(\theta) \quad (1)$$

where ϵ represents random noise with scale γ . Given the training data $\mathcal{D} := \{\mathbf{x}, \mathbf{y}\}$, we can estimate the posterior distribution of the model's parameters $p(\theta|\mathcal{D})$ by Bayesian inference. Since the true posterior is often intractable, an approximate distribution $q(\theta)$ is obtained by minimizing the following the Kullback-Leibler divergence (KL-divergence) [21], [22]:

$$\underset{\theta}{\text{minimize}} \text{KL}[q(\theta) \parallel p(\theta|\mathcal{D})] \quad (2)$$

According to [23], $q(\theta)$ can be represented as a Gaussian distribution for each individual weight θ_s as:

$$q(\theta|\mu_\theta, \sigma_\theta) = \prod_s \mathcal{N}(\theta_s|\mu_s, \sigma_s) \quad (3)$$

where $\theta = \{\theta_s\}$, $\mu_\theta = \{\mu_s\}$, $\sigma_\theta = \{\sigma_s\}$. However, the minimization of the KL-divergence in (2) is still difficult to find for general distributions. Empirically, the prior distribution $p(\theta)$ can be selected as a Gaussian distribution with zero mean and standard deviation $\bar{\sigma}$. Then (2) can be computed as [24]:

$$\begin{aligned} & \min_{\mu_\theta, \sigma_\theta} \frac{1}{2\gamma^2} \mathbb{E}_{q(\theta|\mu_\theta, \sigma_\theta)} \log p(\mathcal{D}|\theta) \\ & + \frac{1}{2\bar{\sigma}^2} (\|\mu_\theta\|^2 + \|\sigma_\theta\|^2) - \sum_s \log\left(\frac{\sigma_s}{\bar{\sigma}}\right) + \text{const.} \end{aligned} \quad (4)$$

2) *Score-based diffusion model*: Diffusion models learn the implicit prior of the underlying data distribution by matching its score function ($\nabla \log_x p(\mathbf{x})$). This prior can be employed for reconstructing images from undersampled measurements through a forward measurement operator and detector noise.

Let $p(\mathbf{x})$ denote an unknown distribution containing samples that follow an independent and identically distributed pattern. Since calculating $\nabla \log_{\mathbf{x}} p(\mathbf{x})$ directly is challenging, the score function can be approximated by a neural network \mathbf{s}_ϕ using the denoising score matching method [25]. Then the samples belonging to $p(\mathbf{x})$ can be obtained via Langevin MCMC sampling according to the following formula:

$$\mathbf{x}_{i+1} = \mathbf{x}_i + \frac{\eta_i}{2} \mathbf{s}_\phi(\mathbf{x}_i) + \sqrt{\eta_i} \mathbf{z}_i \quad (5)$$

where $\eta_i > 0$ represents the step size, and $\mathbf{z}_i \sim \mathcal{N}(\mathbf{0}, \mathbf{I})$.

B. The proposed method

1) *MRI reconstruction model*: Let $\mathbf{X} \in \mathbb{C}^{N_{\text{voxel}} \times N_{\text{mc}}}$ represent a multi-contrast image series to be reconstructed, where each \mathbf{x}_j ($j = 1, 2, \dots, N_{\text{mc}}$) has N_{voxel} voxels. N_{mc} represents the number of contrasts. $\mathbf{Y} \in \mathbb{C}^{N_{\text{voxel}} \times N_c \times N_{\text{mc}}}$ is the k -space data, where \mathbf{y}_j is the measurement for each contrast image, and N_c denotes the number of coils. The reconstruction model to recover \mathbf{X} from its undersampled measurements is typically defined as follows:

$$\arg \min_{\mathbf{X}} \frac{1}{2} \|\mathbf{A}\mathbf{X} - \mathbf{Y}\|_F^2 + \lambda R(\mathbf{X}), \quad (6)$$

where \mathbf{A} represents the encoding operator given by $\mathbf{A} = \mathbf{M}\mathbf{F}\mathbf{S}$, \mathbf{M} is the undersampling operator that undersamples k -space data for each contrast image. \mathbf{F} is the Fourier transform operator, and \mathbf{S} denotes an operator which multiplies the coil sensitivity map with each contrast image coil-wise. $\|\cdot\|_F$ is the Frobenius norm. $R(\mathbf{X})$ denotes a combination of regularizations, and λ is the regularization weight. In conventional compressed sensing (CS) methods, $R(\mathbf{X})$ in (6) denotes a combination of sparse [26], low-rank [8], or other-type of regularization functions. From a Bayesian perspective, $R(\mathbf{X})$ can be considered as the prior model of the data, denoted as $p(\mathbf{X})$. Consequently, it's reasonable to assume that a more precise estimation of this intricate prior data distribution would result in higher-quality samples.

Given that fully sampled \mathbf{X} is inaccessible, we are compelled to explore a label-free method for estimating $p(\mathbf{X})$. To achieve this, a mapping from \mathbf{Y} to \mathbf{X} is firstly estimated, and then $p(\mathbf{X})$ is approximated to characterize the correlation among the MC images.

2) *Self-supervised Bayesian reconstruction network*: Let \mathbf{Y} and \mathbf{X} denote the undersampled k -space data and the corresponding MR image, respectively. A secondary sub-sampling mask is applied to the measurements, resulting in $\mathbf{Y}' = \mathbf{M}'\mathbf{Y}$. A BCNN can be trained using the sub-sampled data \mathbf{Y}' and the zero-filling image \mathbf{X}' of \mathbf{Y} to embody the representation \mathbf{f}_θ with network parameter θ :

$$\mathbf{X}' = \mathbf{f}_\theta(\mathbf{Y}') + \mathbf{n}_1 \quad (7)$$

Then the established transformation is utilized to convert the measured \mathbf{Y} to its corresponding image \mathbf{X} :

$$\mathbf{X} = \mathbf{f}_\theta(\mathbf{Y}) + \mathbf{n}_2 \quad (8)$$

where \mathbf{n}_1 and \mathbf{n}_2 represent Gaussian noise with scales γ_1 and γ_2 . To train the BCNN, we first initialize the parameter θ

from a normal Gaussian noise distribution $\epsilon \sim \prod_s \mathcal{N}(\epsilon_s | 0, 1)$, where ϵ_s denotes the s -th element of ϵ . Subsequently, θ can be sampled through the reparameterization, i.e. $\theta = \mu_\theta + \sigma_\theta \epsilon$. Assuming that the measurement noise \mathbf{n}_1 follows Gaussian white noise, i.e., $p(\mathbf{n}_1) \sim \prod_t \exp\left(-\frac{n_t^2}{2\gamma_1^2}\right)$, and that the prior $p(\theta) \sim \prod_s \exp\left(-\frac{\theta_s^2}{2\sigma^2}\right)$, the minimum of the KL divergence in (4) can be calculated by:

$$\begin{aligned} \min_{\mu_\theta, \sigma_\theta} \frac{1}{2\gamma_1^2} \mathbb{E}_{q(\theta | \mu_\theta, \sigma_\theta)} \sum_{i=1}^N \|\mathbf{f}_\theta(\mathbf{X}'_i) - \mathbf{Y}_i\|_2^2 \\ + \frac{1}{2\sigma^2} (\|\mu_\theta\|_2^2 + \|\sigma_\theta\|_2^2) - \sum_s \log \frac{\sigma_s}{\bar{\sigma}} + \text{const.} \end{aligned} \quad (9)$$

where N represents the number of training datasets.

3) *MC image reconstruction via score-based model with joint distribution*: Utilizing the above estimated $q(\theta)$, we can derive the distribution $p(\mathbf{X} | \mathcal{D})$ using the Bayesian equation:

$$p(\mathbf{X} | \mathcal{D}) = \int p(\mathbf{X} | \mathbf{Y}, \theta) \prod_{j=1}^{N_{\text{mc}}} p(\mathbf{y}_j) q(\theta) d\mathbf{Y} d\theta \quad (10)$$

Since evaluating the integral in (10) is computationally complex, we employ the score matching technique to approximate $\nabla \log_{\mathbf{X}} p(\mathbf{X})$. The fundamental concept behind score matching [27] is to optimize the parameters ϕ of the score-matching network in such a way that $\mathbf{s}_\phi(\mathbf{X}; \theta) = \nabla \log q(\mathbf{X}; \theta)$ closely matches the corresponding score of the true distribution, namely $\nabla \log p(\mathbf{X})$. The objective function to minimize is the expected squared error between these two, expressed as: $\mathbb{E}_{p(\mathbf{X})} \left[1/2 \|\mathbf{s}_\phi(\mathbf{X}) - \nabla \log p(\mathbf{X})\|^2 \right]$. Importantly, this objective is equivalent to the following denoising score matching objective:

$$\min_{\phi} \mathbb{E}_{p(\mathbf{X}, \mathbf{Y}, \theta)} \left[\frac{1}{2} \left\| \mathbf{s}_\phi(\mathbf{X}) - \frac{\partial \log p(\mathbf{X} | \theta, \mathbf{Y})}{\partial \mathbf{X}} \right\|^2 \right] \quad (11)$$

The fundamental concept here is that the gradient $\mathbf{s}_\phi(\mathbf{X})$ of the log density at different corrupted points $\tilde{\mathbf{X}}$ should ideally guide us toward the clean sample \mathbf{X} . More precisely, we perturb $\mathbf{f}_\theta(\mathbf{Y})$ by Gaussian noise with different scales $\{\varepsilon_i\}_{i=1}^L$ which satisfies $\varepsilon_1 < \varepsilon_2 < \dots < \varepsilon_L$. Let $p_{\varepsilon_i}(\tilde{\mathbf{X}} | \mathbf{Y}, \theta) = \mathcal{N}(\tilde{\mathbf{X}} | \mathbf{f}_\theta(\mathbf{Y}), \varepsilon_i^2 \mathbf{I})$, and the corrupted data distribution can be expressed as $p_{\varepsilon_i}(\tilde{\mathbf{X}}) = \int p_{\varepsilon_i}(\tilde{\mathbf{X}} | \mathbf{Y}, \theta) p(\mathbf{Y}) q(\theta) d\mathbf{Y} d\theta$. It can be observed that $p_{\varepsilon_1}(\tilde{\mathbf{X}}) = p(\mathbf{X})$ when $\varepsilon_1 = \gamma_2$. We can estimate the scores of all corrupted data distributions $\{\varepsilon_i\}_{i=1}^L$: $\mathbf{s}_\phi(\mathbf{X}, \varepsilon_i) \approx \nabla \log p_{\varepsilon_i}(\tilde{\mathbf{X}})$. This is achieved by training the joint score function with the following objective:

$$\frac{1}{2L} \sum_{i=1}^L \mathbb{E}_{p(\mathbf{Y}) q(\theta)} \mathbb{E}_{p_{\varepsilon_i}(\tilde{\mathbf{X}} | \mathbf{Y}, \theta)} \left[\left\| \varepsilon_i \mathbf{s}_\phi(\tilde{\mathbf{X}}, \varepsilon_i) + \frac{\tilde{\mathbf{X}} - \mathbf{f}_\theta(\mathbf{Y})}{\varepsilon_i} \right\|^2 \right] \quad (12)$$

After the score function is estimated, the Langevin MCMC sampling can be applied to reconstruct MC images via the

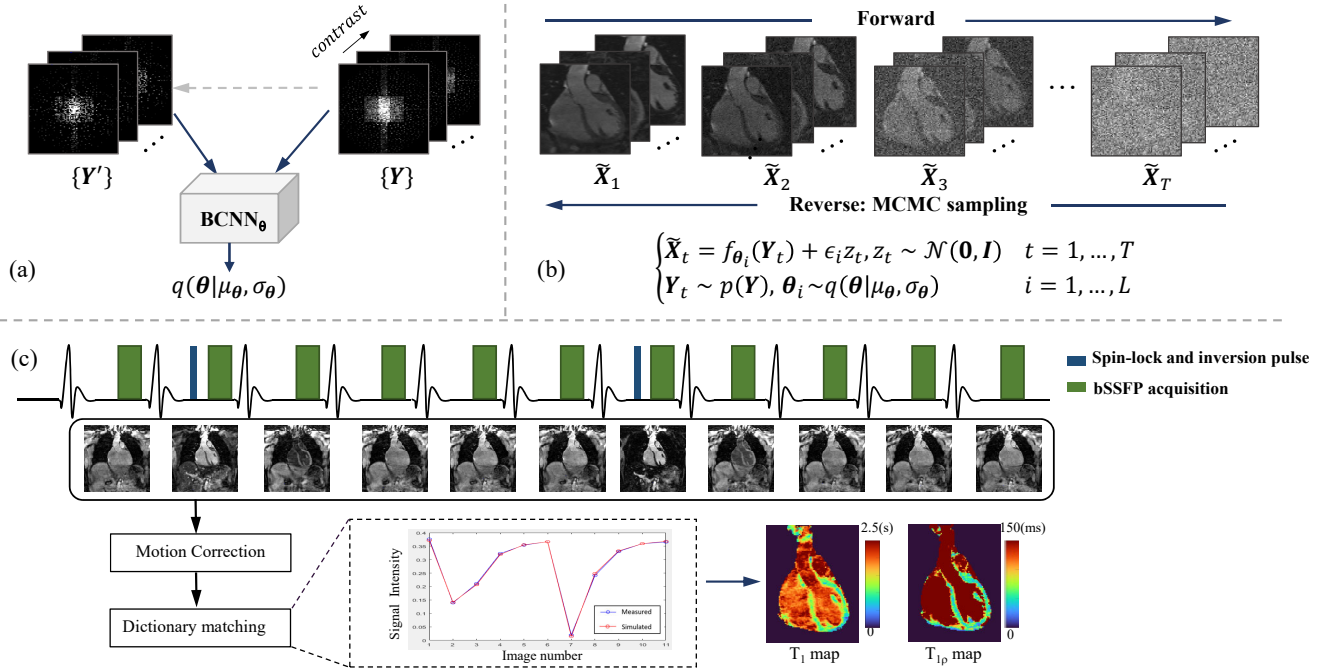


Fig. 1. Illustration of the proposed approach. (a) Flowchart illustrating the self-supervised BCNN for modeling the parameter distribution. BCNN takes undersampled k -space data pairs $\{Y, Y'\}$ as input, and produces $q(\theta|\mu_\theta, \sigma_\theta)$ as an approximation of $q(\theta|\mathcal{D})$. (b) Forward and reverse diffusion processes of the score-based model. In the forward process, the score function, approximating the probability density gradient of X , is learned by perturbing data $f_\theta(X)$ with multiple noise scales. In the reverse process, multi-contrast images are reconstructed by generating samples from the probability density $p(X)$ using Langevin MCMC sampling conditioned on the measurement Y . (c) Diagram of the pulse sequence and post-processing steps used to estimate T_1 and $T_{1\rho}$ maps via the dictionary matching technique.

following formula:

$$\begin{aligned}
 \tilde{X}_{i+1} &= \tilde{X}_i + \frac{\eta_i}{2} \nabla \log p(\tilde{X}_i|Y) + \sqrt{\eta_i} z_i \\
 &= \tilde{X}_i + \frac{\eta_i}{2} (\nabla \log p(\tilde{X}_i) + \nabla \log p(Y|\tilde{X}_i)) + \sqrt{\eta_i} z_i \\
 &= \tilde{X}_i + \frac{\eta_i}{2} (s_\phi(\tilde{X}_i, \epsilon_i) + \frac{\mathbf{A}^H(\mathbf{A}\tilde{X}_i - Y)}{\gamma^2 + \epsilon_i^2}) + \sqrt{\eta_i} z_i
 \end{aligned} \tag{13}$$

where η_i serves as the step size. The specific values of η_i used in this study adhere to those outlined in [28], and the complete sampling procedure is shown in Algorithm 1.

Algorithm 1 Conditional Langevin MCMC Sampling.

- 1: **Input:** $\{\epsilon_i\}_{i=1}^L, \epsilon$ and T ;
 - 2: **Initialize:** \tilde{X}_0 ;
 - 3: **for** $i = 1, \dots, L$ **do**
 - 4: $\eta_i = \epsilon \cdot \epsilon_i^2 / \epsilon_L^2$
 - 5: **for** $t = 1, 2, \dots, T$ **do**
 - 6: Draw $z_t \sim \mathcal{N}(\mathbf{0}, \mathbf{I})$;
 - 7: $\tilde{X}_t = \tilde{X}_{t-1} + \frac{\eta_i}{2} (s_\phi(\tilde{X}_{t-1}, \epsilon_i) + \frac{\mathbf{A}^H(\mathbf{A}\tilde{X}_{t-1} - Y)}{\gamma^2 + \epsilon_i^2}) + \sqrt{\eta_i} z_t$
 - 8: **end for**
 - 9: $\tilde{X}_0 = \tilde{X}_T$
 - 10: **end for**
 - 11: **Output:** \tilde{X}_T .
-

C. Implementation details

Figure 1 illustrates the SSJDM framework. This framework comprises three main components: (a) the BCNN network, (b) the score matching network, and (c) the joint T_1 and $T_{1\rho}$ mapping sequence and the parametric maps estimation procedure. In this section, we focus on the implementation specifics of the BCNN and the score matching network [29].

The BCNN network comprises 10 blocks. Each block (as shown in Figure 2) consists of both an upper and a lower module. The upper module exploits redundancy in the image domain, while the lower module ensures inherent self-consistency in the k -space. Each upper and lower module comprises four sequential convolution layers, each followed by a ReLU activation layer, and a Bayesian convolution layer. Notably, f_θ and the distribution of θ together form the BCNN with an output channel count of $N_c \times N_{mc} \times 2$.

We used NCSNv2 framework in [28] as the score matching network. The network input and output have $N_{mc} \times 2$ channels. To establish the joint distribution, the MC images were reshaped so that the input data size of network is $N_b \times (N_{mc} \times 2) \times N_z \times N_y$, where N_b denotes the batch size, N_z and N_y denote the number of in the partition and phase encoding lines, respectively.

III. EXPERIMENTS

A. Data acquisition

We utilized a 3D simultaneous cardiac T_1 and $T_{1\rho}$ mapping sequence on a 3T MR scanner (uMR 790, United Imaging

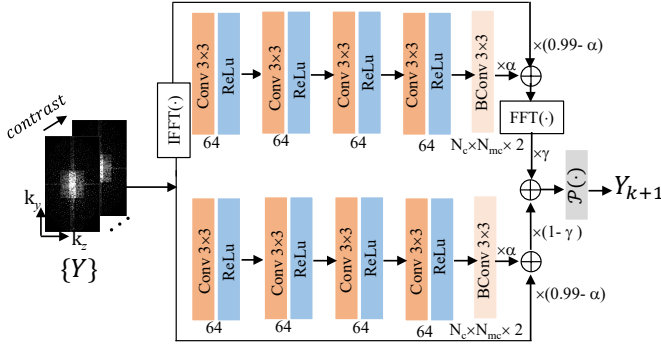


Fig. 2. The network Structure of one block in f_{θ} used in the proposed method. The operators $\text{FFT}(\cdot)$ and $\text{IFFT}(\cdot)$ represent the Fourier and inverse Fourier transforms, respectively. $\mathcal{P}(\cdot) = (I - M')(\cdot) + Y'$ denotes projection onto Y' .

Healthcare, Shanghai, China) equipped with 12-channel cardiac and 48-channel spine coils. This sequence, as depicted in Figure 1(c), closely resembles the one in [7] and incorporates an image-based navigator (iNAV) for respiratory motion correction. Prior to the employed readout of the bSSFP, we introduced an adiabatic constant amplitude spin-lock preparation pulse [30] to create the $T_{1\rho}$ contrast. After $T_{1\rho}$ preparation, the magnetization is tipped down to the $-z$ axis and the acquired signals during magnetization recovery encompass both T_1 and $T_{1\rho}$ weightings.

We prospectively undersampled the 3D-MC-CMR dataset using the above sequence, employing a variable-density Poisson-disc undersampling mask with an acceleration rate of $R = 6$. The 24×24 k -space center was fully sampled for coil sensitivity estimation. Imaging parameters were: shot number = 60, matrix = $176 \times 172 \times 72$, resolution = $1 \times 1 \times 1$ mm³, and TR/TE = 3.28/1.64 ms. Each dataset contained 11 images acquired in three parts: the first image was acquired without the preparation pulse; the second part applied the preparation pulse with a spin-lock time (TSL) of 30 ms and an inversion time (TI) of 0 ms, followed by the acquisition of k -space segments of 5 images (one per heartbeat) and 3 additional heartbeats for magnetization recovery; the third part was the same as the second, except with TSL = 60 ms and TI = 100 ms. The average acquisition time for each dataset was around 18-19 minutes, depending on the volunteers' heartbeats. The coil number varied between 20 and 24, depending on the choice of coils in the heart and spine. The coil sensitivity maps were estimated from the fully sampled k -space center using ESPiRiT [31], with a kernel size of 6×6 , as well as thresholds of 0.02 and 0.95 for calibration-matrix and eigenvalue decomposition.

Each 3D k -space dataset was split into 2D slices along the frequency encoding direction by applying the inverse Fourier transform in that direction. The first 30 and last 20 slices were excluded due to the absence of coverage in the cardiac region. The training set consisted of 5796 slices from 46 volunteers (126 slices per volunteer), while the test set included 1512 slices from 12 volunteers.

B. Reconstruction experiments

To evaluate the proposed method, the test data were retrospectively undersampled using a 2D Poisson-disc sampling pattern with net acceleration rates of $R = 11$ and 14. The proposed SSJDM was used to reconstruct the MC images. Subsequently, T_1 and $T_{1\rho}$ maps were estimated from the reconstructed images using the dictionary matching method described later. The results were compared with those obtained using traditional regularized reconstruction (PROST [32]), a self-supervised DL method (SSDU [12]), and BCNN.

For SSJDM, the BCNN network was configured with $\alpha = 0.5$ and $\gamma = 0.5$. The score matching network employed parameters $\varepsilon_1 = 0.01$, $\varepsilon_L = 50$, $L = 266$, $T = 4$, and exponential moving averages (EMA) were enabled with an EMA rate of 0.999. Both networks were trained using the Adam optimizer, with a learning rate of 10^{-4} , over 500 epochs, optimizing the respective loss functions in (9) and (12), with a batch size of 1. For the PROST method, the parameters included a conjugate gradient tolerance of 10^{-5} , a maximum of 15 CG iterations, a penalty parameter $\mu = 0.08$, regularization parameter for high-order singular value decomposition of 0.01, and a maximum of 10 alternating direction method of multipliers iterations. The SSDU method employed a loss mask ratio of 0.4, and used the Adam optimizer with a learning rate of 10^{-5} , and had a batch size of 1 during 100 epochs of training. SSJDM and SSDU experiments were conducted using PyTorch 1.10 and TensorFlow 2.10 in Python, respectively, on a workstation equipped with an Ubuntu 20.04 operating system, an Intel E5-2640V3 CPU (2.6 GHz, 256 GB memory), and an NVIDIA Tesla A100 GPU with CUDA 11.6 and CUDNN support. PROST reconstruction was implemented in MATLAB (R2021a, MathWorks, Natick, MA).

Additionally, the performance of SSJDM, PROST, SSDU, and BCNN methods was evaluated on prospectively undersampled k -space data acquired from two volunteers with $R = 11$ and 14.

C. T_1 and $T_{1\rho}$ estimation

T_1 and $T_{1\rho}$ parametric maps were generated using the dictionary matching method [33]. The dictionary comprised simulated MR signal evolutions generated via Bloch simulation with the imaging parameters as well as the predefined ranges of T_1 , T_2 , and $T_{1\rho}$ values. Subject-specific dictionaries were simulated based on recorded R-R intervals and trigger delays for each scan. The dictionary for this study included 410550 atoms, covering combinations of T_1 in [50:20:700, 700:10:900, 900:5:1300, 1300:50:3000] ms, $T_{1\rho}$ in [5:5:20, 20:0.5:60, 60:5:100, 100:10:300] ms, and T_2 in [40:0.5:50] ms, with the notation [lower value: step size: upper value]. Image registration was employed to align the myocardial region in the MC images before dictionary matching. Subsequently, T_1 and $T_{1\rho}$ maps were estimated using the pixel-wise dictionary matching. Reference 2D cardiac T_1 and $T_{1\rho}$ maps were obtained using MOLLI [34] and 5-point $T_{1\rho}$ mapping sequences [30], respectively.

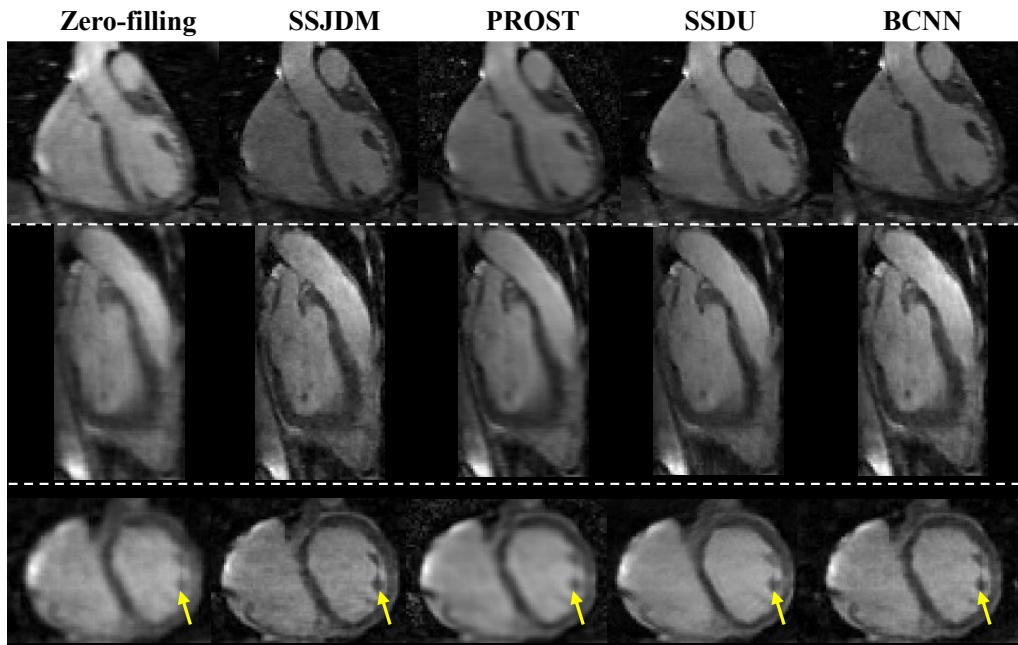


Fig. 3. Reconstructed images using SSJDM, and the zero-filling, PROST, SSDU, BCNN methods with an acceleration rate of $R = 6$. Images of PROST exhibit noticeable blurring, and images of SSJDM show sharper papillary muscles than those of SSDU and BCNN (indicated by the yellow arrows).

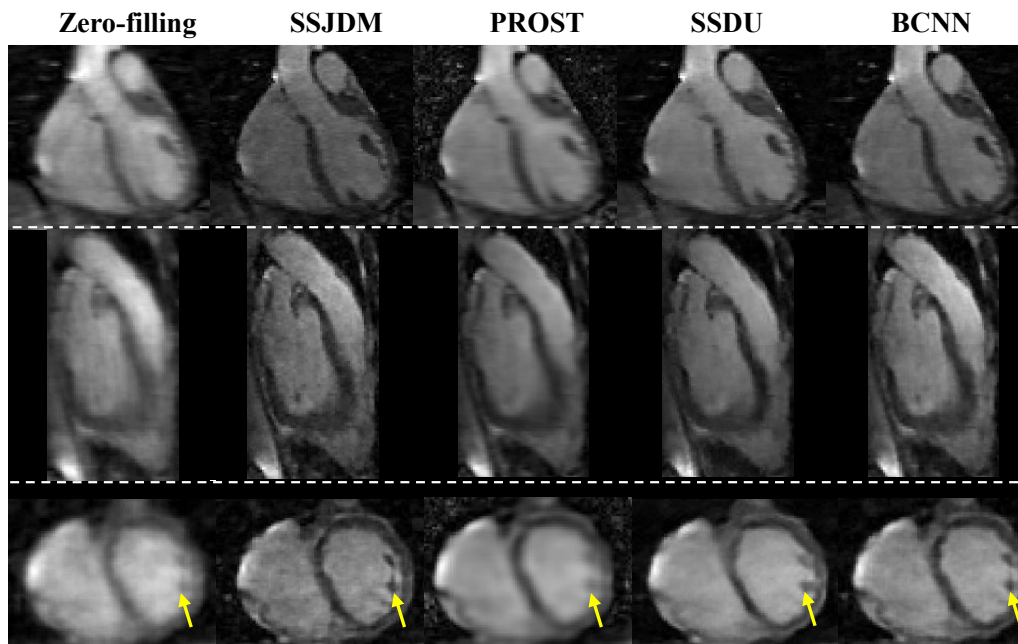


Fig. 4. Reconstructed images using SSJDM, and the zero-filling, PROST, SSDU, BCNN methods with an acceleration rate $R = 11$. Blurring artifacts of PROST become evident. BCNN preserves more detailed information than SSDU (i.e., the papillary muscle area indicated by the yellow arrows). Images of SSJDM still exhibit sharp boundaries and high texture fidelity.

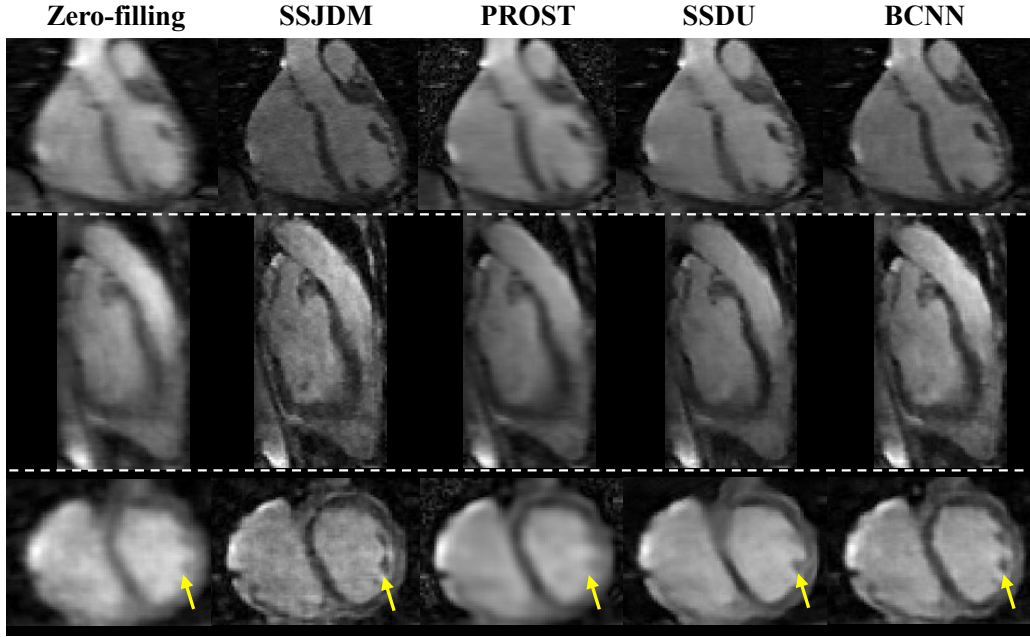


Fig. 5. Reconstructed images using SSJDM, and the zero-filling, PROST, SSDU, BCNN methods with an acceleration rate $R = 14$. The yellow arrows show the papillary muscle areas in the reconstructed images. Even at a high acceleration rate of $R = 14$, the image quality of SSJDM degrades a little, while other methods exhibit severe blurring artifacts.

D. Ablation studies

We conducted three ablation studies to assess the impact of the BCNN network and the joint score-based model on reconstruction performance.

1) *Ablation study 1*: To evaluate the impact of BCNN, we trained the score matching network using MC images reconstructed through conventional CS with total variance (TV) regularization [35].

2) *Ablation study 2*: Similar to the first ablation study, we also trained the score matching network using images reconstructed with the SSDU network.

3) *Ablation study 3*: To investigate the impact of the joint distribution in the score-based model, we employed a score-based model with the traditional independent distribution for reconstruction, and compared the results with SSJDM.

IV. RESULTS

Figure 3 shows MC images from one volunteer, reconstructed using the SSJDM, PROST, SSDU, and BCNN methods at $R = 6$. Zero-filling reconstructions are also presented. Among the reconstructed results, the images of PROST exhibit noticeable blurring. The rest three methods successfully reconstructed images at this acceleration rate, while the images of SSJDM show sharper papillary muscles than those of SSDU and BCNN (indicated by the yellow arrows). Figure 4 shows the reconstructed results using the four methods at $R = 11$. Blurring artifacts of PROST become noticeable in scenarios with higher acceleration rates. BCNN preserves more detailed information than SSDU, notably in the reconstructed papillary muscle area (indicated by the yellow arrows), since it can be treated as an improved version of SSDU [17]. Images of SSJDM still exhibit sharp boundaries and high texture

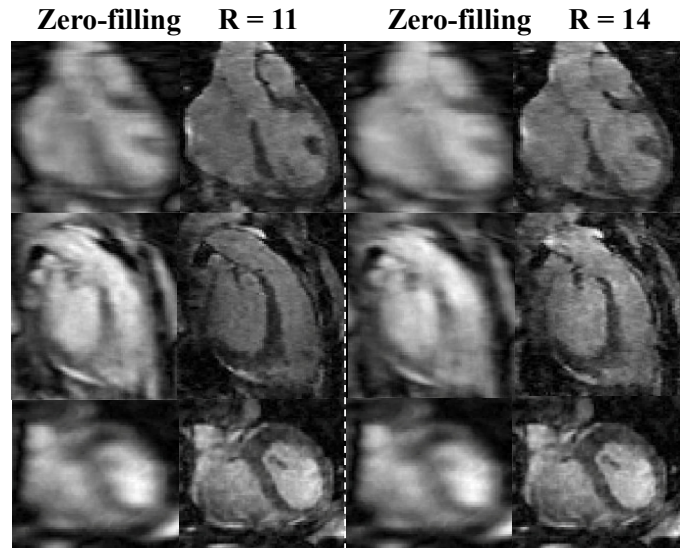


Fig. 6. Images reconstructed using SSJDM and the zero-filling images reconstructed from prospectively undersampled datasets at $R = 11$ and 14.

fidelity, highlighting the superior performance of score-based reconstruction methods in restoring image details. At an even higher acceleration rate of $R = 14$ (shown in Figure 5), the image quality of SSJDM degrades a little, while other methods exhibit severe blurring artifacts.

Figure 6 shows reconstructed images using SSJDM and zero-filling images from the prospectively undersampled datasets at $R = 11$ and 14, which further confirms the effectiveness of the proposed SSJDM method for 3D-MC-CMR reconstruction.

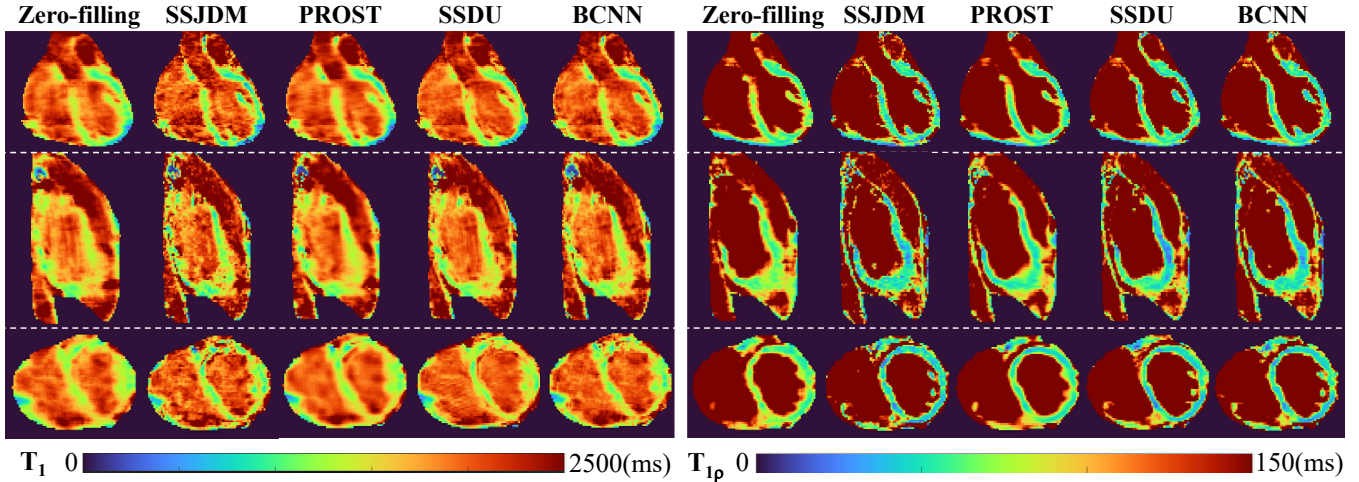


Fig. 7. T_1 and $T_{1\rho}$ maps estimated from reconstructed images using the proposed method, and the zero-filling, PROST, SSDU, BCNN methods with acceleration rate $R = 11$. The maps of SSJDM exhibit sharp boundaries and high texture fidelity.

Figure 7 shows the T_1 and $T_{1\rho}$ maps estimated from reconstructions using different methods at $R = 11$. Similar conclusions can be drawn from the estimated maps as those from the reconstructed MC images at the same acceleration rate shown in Figure 4. The 3D T_1 , $T_{1\rho}$ maps of SSJDM at $R = 6$ and $R = 11$ are also reformatted to 2D slices in the standard short-axis (SAX) view of the heart, and compared with the reference 2D maps obtained from MOLLI and $T_{1\rho}$ mapping sequences (shown in Figure 8). The pseudo colors of the myocardium using SSJDM are quite close to those of the references, indicating they have similar values. Table I shows the mean and standard deviation of T_1 , $T_{1\rho}$ values using SSJDM in manually drawn myocardium regions at different acceleration rates and the reference values. The estimated T_1 and $T_{1\rho}$ values of SSJDM are consistent with the reference values.

Figure 9 shows reconstructed images at $R = 6$, 11, and 14 using SSJDM and the methods from three ablation studies. Ablation 1 exhibits severe noise, attributed to the training data originating from conventional CS, which is prone to substantial noise amplification at higher acceleration rates [12]. Although noise is effectively mitigated by substituting the input data with reconstructions from the SSDU method, the resulting images (referred to as "Ablation 2") still display blurriness, especially at higher acceleration rates, such as $R = 14$. Images reconstructed using the independent distribution (referred to as "Ablation 3") exhibit slight blurring compared to SSJDM, indicating an enhanced reconstruction quality with the joint distribution.

TABLE I

THE ESTIMATED MYOCARDIAL T_1 AND $T_{1\rho}$ VALUES (MEAN \pm STD, UNIT:MS) AT DIFFERENT ACCELERATION RATES USING SSJDM COMPARED WITH THE REFERENCE VALUES

	Reference	R = 6	R = 11	R = 14
T_1	1080.42 \pm 25.65	1040.24 \pm 31.24	1045.06 \pm 39.46	1034.56 \pm 33.01
$T_{1\rho}$	61.36 \pm 1.53	60.98 \pm 3.04	62.06 \pm 4.00	63.90 \pm 4.42

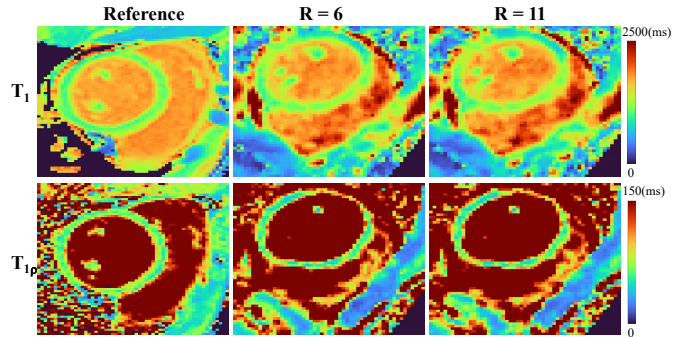


Fig. 8. T_1 and $T_{1\rho}$ maps estimated from SSJDM at $R = 6$ and 11 using the dictionary matching method, and the reference maps from the MOLLI and $T_{1\rho}$ mapping sequences.

V. DISCUSSION

In this study, we proposed the SSJDM method, which utilizes a self-supervised BCNN to train the score-based model without the need for high-quality training data. This approach enabled the successful reconstruction of MC images from highly undersampled k -space data. We have shown that our method can mitigate the discrepancy between the output of single-model-based methods (i.e., CS-based or generally deterministic networks-based methods) and actual data, since this method considers the stochastic nature of parameters in the reconstruction model. This enhancement leads to improved image quality of the score-based model, resulting in superior performance compared to self-supervised SSDU and BCNN approaches. The SSJDM method demonstrated favorable reconstructions in 3D cardiac imaging. It allowed for the simultaneous estimation of T_1 and $T_{1\rho}$ parametric maps in a single scan. Moreover, the estimated T_1 and $T_{1\rho}$ parameter values exhibited a strong consistency with those obtained from conventional 2D imaging.

Acquiring high-quality training samples is super challenging in MRI, especially in 3D cardiac imaging. The fully sampled acquisition for the 3D-MC-CMR imaging sequence in this

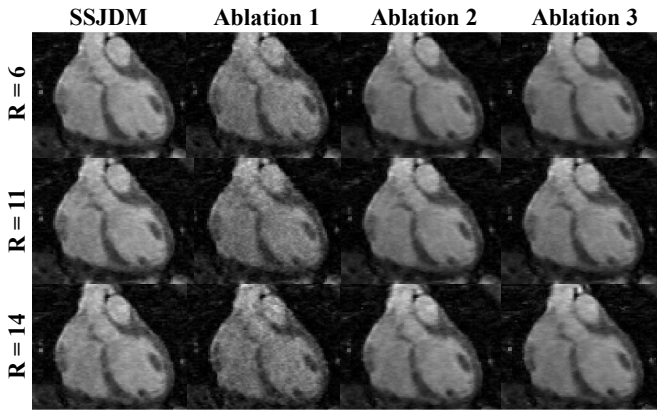


Fig. 9. Reconstructed images at different acceleration rates in the ablation studies. Images of Ablation 1 exhibit severe noise, and images of Ablation 2 and Ablation 3 exhibit blurring compared to those of SSJDM.

study would be over 2 hours. This prolonged scan duration could easily induce subject motion, leading to motion artifacts. Therefore, conventional supervised reconstruction techniques are no longer suitable for such scenarios. Unsupervised learning-based imaging techniques, including self-supervised, untrained, and unpaired learning approaches, may provide an alternative to tackle this challenge. Untrained imaging methods, such as traditional CS-based methods [26], untrained neural network-based methods like deep image prior (DIP) [36], and k -space interpolation with untrained neural network (K-UNN) [37], do not rely on training data and have exhibited remarkable performance. However, CS-based methods have computationally intensive processes, and optimizing the regularization parameters is non-trivial. Untrained neural network-based methods rely on the neural network structure for implicit regularization and face challenges in selecting an appropriate regularization parameter and early stopping condition when fitting the network to the given undersampled measurement. Unpaired deep learning approaches based on generative models, such as variational autoencoders [38], generative adversarial networks [39], normalizing flows [40], and the original diffusion model [41], have been introduced for MR image reconstruction. The related networks are typically trained without paired label data. However, the training process for these approaches still requires fully sampled datasets, making them different from our study and unsuitable to our application scenario. Therefore, we undertake the reconstruction of 3D-MC-CMR images in a self-supervised learning manner.

In ablation studies, we observed a degradation in reconstruction quality when training the score matching network with images reconstructed through conventional CS method. As mentioned in previous literatures, higher factors can lead to degradation in CS reconstructions, which in turn impact the performance of the trained score matching network. Employing training datasets generated by a more effective method, such as the SSUD method, can improve the reconstruction performance of the score matching network. However, the improvement is restricted because the SSDU method learns

the transportation mapping with deterministic weights. Either CS or SSDU approach entails the use of a single model or a network with fixed parameters to reconstruct training samples for the score matching network. However, these approaches may fall short in adequately capturing the diversity inherent in real data. The BCNN provides a natural approach to quantify uncertainty in deep learning [17], i.e., leveraging a set of models or parameters to comprehensively represent the diversity within real data can effectively serve the purpose of ensemble learning. In this study, the proposed SSJDM method learns the transportation mapping built on the framework of Bayesian neural network with the weights treated as random variables following a certain probability distribution. In contrast, in ablation studies 1 and 2, the input data correspond to a learned transportation mapping with deterministic weights. Consequently, this self-supervised BCNN training seems to enhance the network’s generalization capacity, and this learning strategy holds potential for further improving the reconstruction performance.

There are several limitations in this study. Firstly, the SSJDM method consumes much longer reconstruction time than end-to-end DL-based reconstruction methods. This limit is inherited from a major drawback of score-based generative models, which require large sampling steps of the learned diffusion process to reach the desired accuracy. Amounts of sampling-acceleration strategies have been proposed, such as consistency models [42], ordinary differential equation solver [43], and demonstrated that similar sampling results can be achieved even within less than ten steps. However, most of their performance has not yet been evaluated in MR reconstruction. We aim to explore these sampling-acceleration strategies in our future work to reduce the reconstruction time of the SSJDM method, making it more suitable for clinical use. Secondly, dictionary-matching for T_1 and $T_{1\rho}$ estimation is another time-consuming procedure, depending on dictionary size and pixel count. Techniques, like dictionary compression [44] and DL network for direct mapping [45], [46], offer potential solutions to address this challenge. As this study focuses on reconstructing 3D CMR images, we’ll investigate the fast parameter estimation method in the future.

VI. CONCLUSIONS

This work shows the feasibility of score-based models for reconstructing 3D-MC-CMR images from highly undersampled data in simultaneous whole-heart T_1 and $T_{1\rho}$ mapping. The proposed method is trained in a self-supervised manner and therefore particularly suited for 3D CMR imaging that lacks fully sampled data. Experimental results showed that this method could achieve a high acceleration rate of up to 14 in simultaneous 3D whole-heart T_1 and $T_{1\rho}$ mapping.

REFERENCES

- [1] S. Rao, S. Y. Tseng, A. Pednekar, S. Siddiqui, M. Kocaoglu, M. Fares, S. M. Lang, S. Kuttly, A. B. Christopher, L. J. Olivieri *et al.*, “Myocardial parametric mapping by cardiac magnetic resonance imaging in pediatric cardiology and congenital heart disease,” *Circ. Cardiovas. Imag.*, vol. 15, no. 1, p. e012242, 2022.

- [2] M. Akçakaya, S. Weingärtner, T. A. Basha, S. Roujol, S. Bellm, and R. Nezafat, "Joint myocardial T_1 and T_2 mapping using a combination of saturation recovery and T_2 -preparation," *Magn. Reson. Med.*, vol. 76, no. 3, pp. 888–896, 2016.
- [3] C. Velasco, G. Cruz, B. Lavin, A. Hua, A. Fotaki, R. M. Botnar, and C. Prieto, "Simultaneous T_1 , T_2 , and $T_{1\rho}$ cardiac magnetic resonance fingerprinting for contrast agent-free myocardial tissue characterization," *Magn. Reson. Med.*, vol. 87, no. 4, pp. 1992–2002, 2022.
- [4] A. G. Christodoulou, J. L. Shaw, C. Nguyen, Q. Yang, Y. Xie, N. Wang, and D. Li, "Magnetic resonance multitasking for motion-resolved quantitative cardiovascular imaging," *Nat. Biomed. Eng.*, vol. 2, no. 4, pp. 215–226, 2018.
- [5] G. Cruz, O. Jaubert, H. Qi, A. Bustin, G. Milotta, T. Schneider, P. Koken, M. Doneva, R. M. Botnar, and C. Prieto, "3D free-breathing cardiac magnetic resonance fingerprinting," *NMR Biomed.*, vol. 33, no. 10, p. e4370, 2020.
- [6] B. Zhao, W. Lu, T. K. Hitchens, F. Lam, C. Ho, and Z.-P. Liang, "Accelerated mr parameter mapping with low-rank and sparsity constraints," *Magn. Reson. Med.*, vol. 74, no. 2, pp. 489–498, 2015.
- [7] G. Milotta, G. Ginami, A. Bustin, R. Neji, C. Prieto, and R. M. Botnar, "3D whole-heart free-breathing qBOOST- T_2 mapping," *Magn. Reson. Med.*, vol. 83, no. 5, pp. 1673–1687, 2020.
- [8] T. Zhang, J. M. Pauly, and I. R. Levesque, "Accelerating parameter mapping with a locally low rank constraint," *Magn. Reson. Med.*, vol. 73, no. 2, pp. 655–661, 2015.
- [9] A. Phair, G. Cruz, H. Qi, R. M. Botnar, and C. Prieto, "Free-running 3D whole-heart T_1 and T_2 mapping and cine mri using low-rank reconstruction with non-rigid cardiac motion correction," *Magn. Reson. Med.*, vol. 89, no. 1, pp. 217–232, 2023.
- [10] E. Martín-González, E. Alskaf, A. Chiribiri, P. Casaseca-de-la Higuera, C. Alberola-López, R. G. Nunes, and T. Correia, "Physics-informed self-supervised deep learning reconstruction for accelerated first-pass perfusion cardiac mri," in *Proc. Int. Conf. Med. Image Comput. Comput.-Assist. Intervent. Workshop*. Springer, 2021, pp. 86–95.
- [11] F. Liu, R. Kijowski, G. El Fakhri, and L. Feng, "Magnetic resonance parameter mapping using model-guided self-supervised deep learning," *Magn. Reson. Med.*, vol. 85, no. 6, pp. 3211–3226, 2021.
- [12] B. Yaman, S. A. H. Hosseini, S. Moeller, J. Ellermann, K. Uğurbil, and M. Akçakaya, "Self-supervised learning of physics-guided reconstruction neural networks without fully sampled reference data," *Magn. Reson. Med.*, vol. 84, no. 6, pp. 3172–3191, 2020.
- [13] B. Zhou, J. Schlemper, N. Dey, S. S. M. Salehi, K. Sheth, C. Liu, J. S. Duncan, and M. Sofka, "Dual-domain self-supervised learning for accelerated non-cartesian MRI reconstruction," *Med. Image Anal.*, vol. 81, p. 102538, 2022.
- [14] Y. Song, C. Durkan, I. Murray, and S. Ermon, "Maximum likelihood training of score-based diffusion models," in *Proc. Int. Conf. Neural Inf. Process. Syst.*, vol. 34, 2021, pp. 1415–1428.
- [15] H. Chung and J. C. Ye, "Score-based diffusion models for accelerated mri," *Med. Image Anal.*, vol. 80, p. 102479, 2022.
- [16] Y. Song, L. Shen, L. Xing, and S. Ermon, "Solving inverse problems in medical imaging with score-based generative models," in *Proc. Int. Conf. Learn. Representations*, 2022.
- [17] L. V. Jospin, H. Laga, F. Boussaid, W. Buntine, and M. Bennamoun, "Hands-on bayesian neural networks—a tutorial for deep learning users," *IEEE Comput. Intell. M.*, vol. 17, no. 2, pp. 29–48, 2022.
- [18] Z.-X. Cui, S. Jia, J. Cheng, Q. Zhu, Y. Liu, K. Zhao, Z. Ke, W. Huang, H. Wang, Y. Zhu *et al.*, "Equilibrated zeroth-order unrolled deep network for parallel mr imaging," *IEEE Trans. Med. Imag.*, 2023.
- [19] M. Henningsson, "Cartesian dictionary-based native T_1 and T_2 mapping of the myocardium," *Magn. Reson. Med.*, vol. 87, no. 5, pp. 2347–2362, 2022.
- [20] W. K. Hastings, "Monte carlo sampling methods using markov chains and their applications," 1970.
- [21] S. Kullback and R. A. Leibler, "On information and sufficiency," *The annals of mathematical statistics*, vol. 22, no. 1, pp. 79–86, 1951.
- [22] E. J. Candès, J. Romberg, and T. Tao, "Robust uncertainty principles: Exact signal reconstruction from highly incomplete frequency information," *IEEE Trans. Inform. Theory*, vol. 52, no. 2, pp. 489–509, 2006.
- [23] A. Graves, "Practical variational inference for neural networks," in *Proc. Int. Conf. Neural Inf. Process. Syst.*, vol. 24, 2011.
- [24] C. M. Bishop and N. M. Nasrabadi, *Pattern recognition and machine learning*. Springer, 2006, vol. 4, no. 4.
- [25] P. Vincent, "A connection between score matching and denoising autoencoders," *Neural Comput.*, vol. 23, no. 7, pp. 1661–1674, 2011.
- [26] M. Lustig, D. Donoho, and J. M. Pauly, "Sparse MRI: The application of compressed sensing for rapid MR imaging," *Magn. Reson. Med.*, vol. 58, no. 6, pp. 1182–1195, 2007.
- [27] A. Hyvärinen and P. Dayan, "Estimation of non-normalized statistical models by score matching," *J. Mach. Learn. Res.*, vol. 6, no. 4, 2005.
- [28] Y. Song and S. Ermon, "Improved techniques for training score-based generative models," in *Proc. Int. Conf. Neural Inf. Process. Syst.*, vol. 33, 2020, pp. 12 438–12 448.
- [29] I. Goodfellow, Y. Bengio, and A. Courville, *Deep learning*. MIT press, 2016.
- [30] Y. Yang, C. Wang, Y. Liu, Z. Chen, X. Liu, H. Zheng, D. Liang, and Y. Zhu, "A robust adiabatic constant amplitude spin-lock preparation module for myocardial $T_{1\rho}$ quantification at 3 T," *NMR Biomed.*, vol. 36, no. 2, p. e4830, 2023.
- [31] M. Uecker, P. Lai, M. J. Murphy, P. Virtue, M. Elad, J. M. Pauly, S. S. Vasanawala, and M. Lustig, "ESPIRiT—an eigenvalue approach to autocalibrating parallel MRI: where SENSE meets GRAPPA," *Magn. Reson. Med.*, vol. 71, no. 3, pp. 990–1001, 2014.
- [32] A. Bustin, G. Ginami, G. Cruz, T. Correia, T. F. Ismail, I. Rashid, R. Neji, R. M. Botnar, and C. Prieto, "Five-minute whole-heart coronary mra with sub-millimeter isotropic resolution, 100% respiratory scan efficiency, and 3D-PROST reconstruction," *Magn. Reson. Med.*, vol. 81, no. 1, pp. 102–115, 2019.
- [33] D. Ma, V. Gulani, N. Seiberlich, K. Liu, J. L. Sunshine, J. L. Duerk, and M. A. Griswold, "Magnetic resonance fingerprinting," *Nature*, vol. 495, no. 7440, pp. 187–192, 2013.
- [34] D. R. Messroghli, A. Radjenovic, S. Kozerke, D. M. Higgins, M. U. Sivananthan, and J. P. Ridgway, "Modified look-locker inversion recovery (MOLLI) for high-resolution T_1 mapping of the heart," *Magn. Reson. Med.*, vol. 52, no. 1, pp. 141–146, 2004.
- [35] L. Feng, R. Grimm, K. T. Block, H. Chandarana, S. Kim, J. Xu, L. Axel, D. K. Sodickson, and R. Otazo, "Golden-angle radial sparse parallel MRI: combination of compressed sensing, parallel imaging, and golden-angle radial sampling for fast and flexible dynamic volumetric MRI," *Magn. Reson. Med.*, vol. 72, no. 3, pp. 707–717, 2014.
- [36] D. Ulyanov, A. Vedaldi, and V. Lempitsky, "Deep image prior," in *Proc. Conf. Comput. Vis. Pattern Recognit.*, 2018, pp. 9446–9454.
- [37] Z.-X. Cui, S. Jia, C. Cao, Q. Zhu, C. Liu, Z. Qiu, Y. Liu, J. Cheng, H. Wang, Y. Zhu *et al.*, "K-UNN: k-space interpolation with untrained neural network," *Med. Image Anal.*, vol. 88, p. 102877, 2023.
- [38] D. P. Kingma and M. Welling, "Auto-encoding variational Bayes," in *Proc. Int. Conf. Learn. Representations*, 2014.
- [39] J.-Y. Zhu, T. Park, P. Isola, and A. A. Efros, "Unpaired image-to-image translation using cycle-consistent adversarial networks," in *Proc. Int. Conf. Comput. Vis.*, 2017, pp. 2223–2232.
- [40] L. Dinh, D. Krueger, and Y. Bengio, "NICE: Non-linear independent components estimation," in *Proc. Int. Conf. Learn. Representations*, 2015.
- [41] J. Ho, A. Jain, and P. Abbeel, "Denoising diffusion probabilistic models," in *Proc. Int. Conf. Neural Inf. Process. Syst.*, vol. 33, 2020, pp. 6840–6851.
- [42] Y. Song, P. Dhariwal, M. Chen, and I. Sutskever, "Consistency models," in *Proc. Int. Conf. Mach. Learn.*, 2023.
- [43] C. Lu, Y. Zhou, F. Bao, J. Chen, C. Li, and J. Zhu, "DPM-solver: A fast ODE solver for diffusion probabilistic model sampling in around 10 steps," in *Proc. Int. Conf. Neural Inf. Process. Syst.*, vol. 35, 2022, pp. 5775–5787.
- [44] D. F. McGivney, E. Pierre, D. Ma, Y. Jiang, H. Saybasili, V. Gulani, and M. A. Griswold, "SVD compression for magnetic resonance fingerprinting in the time domain," *IEEE Trans. Med. Imag.*, vol. 33, no. 12, pp. 2311–2322, 2014.
- [45] O. Cohen, B. Zhu, and M. S. Rosen, "MR fingerprinting deep reconstruction network (DRONE)," *Magn. Reson. Med.*, vol. 80, no. 3, pp. 885–894, 2018.
- [46] Z. Fang, Y. Chen, M. Liu, L. Xiang, Q. Zhang, Q. Wang, W. Lin, and D. Shen, "Deep learning for fast and spatially constrained tissue quantification from highly accelerated data in magnetic resonance fingerprinting," *IEEE Trans. Med. Imag.*, vol. 38, no. 10, pp. 2364–2374, 2019.